AFRL-AFOSR-JP-TR-2018-0045

Electric Current Analysis of Addressable Conducting Network for Damage Monitoring

Akira Todoroki
TOKYO INSTITUTE OF TECHNOLOGY

03/05/2018
Final Report

Air Force Research Laboratory
AF Office Of Scientific Research (AFOSR)/ IOA
Arlington, Virginia 22203
Air Force Materiel Command

FORM SF 298

REPORT DOCUMENTATION PAGE

Form Approved
OMB No. 0704-0188

1. REPORT DATE *(DD-MM-YYYY)*	2. REPORT TYPE	3. DATES COVERED *(From - To)*
24-05-2018	Final	07 Jul 2015 to 06 Jul 2018

4. TITLE AND SUBTITLE
Electric Current Analysis of Addressable Conducting Network for Damage Monitoring

5a. CONTRACT NUMBER

5b. GRANT NUMBER
FA2386-15-1-4090

5c. PROGRAM ELEMENT NUMBER
61102F

6. AUTHOR(S)
Akira Todoroki

5d. PROJECT NUMBER

5e. TASK NUMBER

5f. WORK UNIT NUMBER

7. PERFORMING ORGANIZATION NAME(S) AND ADDRESS(ES)
TOKYO INSTITUTE OF TECHNOLOGY
2-12-1 OOKAYAMA
MEGURO-KU, 152-0033 JP

8. PERFORMING ORGANIZATION REPORT NUMBER

9. SPONSORING/MONITORING AGENCY NAME(S) AND ADDRESS(ES)
AOARD
UNIT 45002
APO AP 96338-5002

10. SPONSOR/MONITOR'S ACRONYM(S)
AFRL/AFOSR IOA

11. SPONSOR/MONITOR'S REPORT NUMBER(S)
AFRL-AFOSR-JP-TR-2018-0045

12. DISTRIBUTION/AVAILABILITY STATEMENT
A DISTRIBUTION UNLIMITED: PB Public Release

13. SUPPLEMENTARY NOTES

14. ABSTRACT
As delamination cracks are usually invisible, it is difficult to identify delamination cracks within carbon-fiber reinforced polymer (CFRP) composite laminates. The difficulties in finding laminate damage by visual inspection raises the need of monitoring methods that use electric resistance changes within the laminates. The method adopts conductive carbon fibers as sensors as well as mechanical reinforcements, that is, in a sense self-sensing. In the present study, the new analysis method is extended to a new electric current arrangement that is used for the addressable conducting network (ACN). The addressable conducting network adopts grid type electrodes mounted on the both sides of the target CFRP laminate in orthogonal direction. Selecting the one electrode on one of the surface and the other on the other surface gives a cross point electric current. The electric current density distribution, however, depends on the fiber direction of each plies. To prevent the high cost computation, the analysis developed by Todoroki is extended in the present study. The analysis enables us to analyze the delamination effect on electric voltage change at various stacking sequences that is needed for optimizations of the direction of the electrode array. The analysis method is adopted for damage monitoring of plate type specimen in the present study, and that method successfully detected the delamination crack.

15. SUBJECT TERMS
AOARD, CFRP, non-destructive

16. SECURITY CLASSIFICATION OF:			17. LIMITATION OF ABSTRACT	18. NUMBER OF PAGES	19a. NAME OF RESPONSIBLE PERSON
a. REPORT	b. ABSTRACT	c. THIS PAGE			KNOPP, JEREMY
Unclassified	Unclassified	Unclassified	SAR	25	19b. TELEPHONE NUMBER *(Include area code)* 315-227-7006

Final/Annual/Midterm Report for AOARD Grant FA2386-15-1-4090

"**Electric Current Analysis for Damage Monitoring**"

5th March 2018

Name of Principal Investigators (PI and Co-PIs): Prof. Akira Todoroki
- e-mail address : atodorok@ginza.mes.titech.ac.jp
- Institution : Tokyo Institute of Technology
- Mailing Address : 2-12-1 (i1-58), Oookayama, Meguro, Tokyo, Japan 1528550
- Phone : +81-3-5734-3178
- Fax : +81-3-5734-3178

Period of Performance: July/07/2015 – July/07/2017

Abstract: As delamination cracks are usually invisible, it is difficult to identify delamination cracks within carbon-fiber reinforced polymer (CFRP) composite laminates. The difficulties in finding laminate damage by visual inspection raises the need of monitoring methods that use electric resistance changes within the laminates. The method adopts conductive carbon fibers as sensors as well as mechanical reinforcements, that is, in a sense self-sensing. In the present study, the new analysis method is extended to a new electric current arrangement that is used for the addressable conducting network (ACN). The addressable conducting network adopts grid type electrodes mounted on the both sides of the target CFRP laminate in orthogonal direction. Selecting the one electrode on one of the surface and the other on the other surface gives a cross point electric current. The electric current density distribution, however, depends on the fiber direction of each plies. To prevent the high cost computation, the analysis developed by Todoroki is extended in the present study. The analysis enables us to analyze the delamination effect on electric voltage change at various stacking sequences that is needed for optimizations of the direction of the electrode array. The analysis method is adopted for damage monitoring of plate type specimen in the present study, and that method successfully detected the delamination crack.

Introduction:

Carbon fiber reinforced polymer (CFRP) laminated composites are used in aircraft, automobiles, and as structural components of other transportation vehicles because of their excellent specific mechanical properties. To prevent delamination cracking of laminated CFRP composites, the use of resin rich layers with elastomer particles has been adopted in the recent highly toughened laminated CFRP [1]. The electrical conductivity of highly toughened CFRP, however, is very low compared with that of conventional laminated CFRP, especially in the through-thickness direction [2]. The electrical conductivity of toughened CFRP is strongly orthotropic, and this may result in structural damage when a lightning strike occurs [3]. As lightning protection, metal foils or meshes are attached to the surface of the CFRP components of in-service aircraft [4]. It is, however, difficult to prevent induced electric current or leaked electric current. Many research articles have addressed the damage of CFRP laminates struck by artificial lightning [2-6]. However, the existence of resin-rich layers in aircraft structures makes it difficult to evaluate electric current distribution in CFRP laminates.

Todoroki previously proposed an analytical method for calculating electric current distribution in laminated CFRP using a newly developed electric potential function for orthotropic laminates [7,8]. The analytical method assumes that CFRPs are homogeneous orthotropic materials. The toughened CFRP laminates used in aircraft, however, are not homogeneous with respect to the through-thickness direction because of their resin-rich layers.

In our previous paper [9], an electrical source and grounding sink couple was placed on the top surface of beam type specimens, and the electric current was experimentally measured and compared with the results of the orthotropic electric potential function analysis. It was found that the equivalent current method was effective and the assumption of the

orthotropic homogeneous materials in the thickness direction was applicable for electric current flowing near the top surface of the laminate. The effectiveness of the method, however, was not confirmed for cases in which the electric current flows mainly in the through-thickness direction.

The objective of the present study is, therefore, to confirm the validity of the orthotropic electric potential analysis method for the through-thickness direction electric current. The equivalent conductivity and the assumption of homogeneity in the through-thickness direction are confirmed for electric current in the through-thickness direction. In the present study, the electric current source and ground (sink) were placed on opposite surfaces of a beam type specimen. The electric current flowed in the oblique line between the current source on the top surface and the grounding sink on the bottom surface. This placement of the electrodes created a large electric current in the through-thickness direction. The electrical potential distribution was also completely different from the distribution observed when the current source and grounding sink couple is placed on the top surface of the specimen, as shown in the previous study [8,9].

A formula for an orthotropic electric potential function was derived for the oblique current path of the beam type specimen in the present study. The oblique electric current path is employed in self-sensing damage monitoring systems of addressable conducting networks [10]. The electric voltage distribution of the oblique electric current path is performed by Selvakumaran et al. [11]. To confirm the validity of the derived formula, comparison with finite element method (FEM) analysis were performed in the present study. The formula is modified for the CFRP laminated plates and a new electric current analysis of delamination crack in a CFRP laminated plate is proposed.

Principle of anisotropic electric potential function analysis:

Anisotropic electric potential function

Let us assume that unidirectional CFRP laminates are orthotropic homogeneous materials electrically. The Cartesian two-dimensional coordinate system of the laminates is defined with the x-axis as the fiber direction and the z-axis as the through-thickness direction. Let the electric conductance of each direction be σ_x and σ_z, respectively. The electric current density in the x- and z-directions (i_x, i_z) can be obtained using the orthotropic electric potential function ϕ as follows:

$$i_x = -\sigma_x \frac{\partial \phi}{\partial x}, \quad i_z = -\sigma_z \frac{\partial \phi}{\partial z} \tag{1}$$

where σ_x and σ_z are the electric conductivity in each direction. For a CFRP laminate, the resin-rich interlamina is neglected and the CFRP laminate is assumed to have uniform electric conductance in the thickness direction. With no electric current input, the equation for the continuity of the electric current is

$$\frac{\partial i_x}{\partial x} + \frac{\partial i_y}{\partial y} = 0 \tag{2}$$

Substitution of equation (1) into equation (2) gives

$$\sigma_x \frac{\partial^2 \phi}{\partial x^2} + \sigma_y \frac{\partial^2 \phi}{\partial y^2} = 0 \tag{3}$$

To deal with the orthotropic coordinate, the following coordinate transformations are adopted

$$\xi = \frac{x}{\sqrt{\sigma_x}}, \ \eta = \frac{z}{\sqrt{\sigma_z}} \tag{4}$$

Using equation (3), the continuity equation becomes

$$\frac{\partial^2 \phi}{\partial \xi^2} + \frac{\partial^2 \phi}{\partial \eta^2} = 0 \tag{5}$$

Equation (5) is the isotropic Laplace equation, which is similar to that for the velocity potential of perfect fluid. This means the potential of a perfect fluid can be applied to the transformed coordinates. Using a couple of a source (electrical source) and sink (electrical ground), the electric potential of the orthotropic conductive material can be analyzed.

Let us consider that an electric current source-sink couple is located on the same surface of this CFRP plate; for definiteness, the source is set at ($-a$, 0) and the sink at (a, 0), where $a>0$ (see Fig. 1). Using the potential flow for this electric source-sink couple, the electric current density can be formulated as

$$i_x = \frac{I}{\pi\sqrt{\sigma_x\sigma_z}}\left\{\frac{x+a}{\frac{(x+a)^2}{\sigma_x}+\frac{z^2}{\sigma_z}} - \frac{x-a}{\frac{(x-a)^2}{\sigma_x}+\frac{z^2}{\sigma_z}}\right\}$$

$$i_z = \frac{I}{\pi\sqrt{\sigma_x\sigma_z}}\left\{\frac{z}{\frac{(x+a)^2}{\sigma_x}+\frac{z^2}{\sigma_z}} - \frac{z}{\frac{(x-a)^2}{\sigma_x}+\frac{z^2}{\sigma_z}}\right\} \quad (6)$$

The details of the orthotropic electric potential theory can be seen in reference [7].

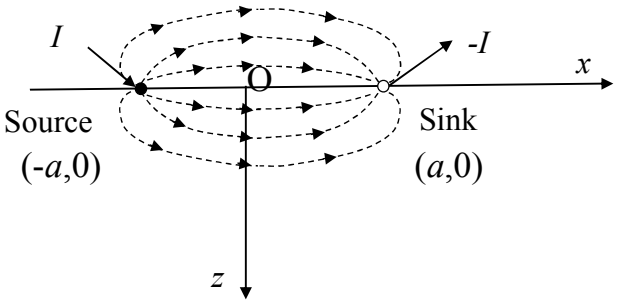

Fig.1 Electric source and sink on an infinite plate.

Mirror image method

The orthotropic electric potential gives the electrical potential distribution and electrical current in an infinite plate. To obtain those for a finite plate (thickness is t, and length is L), a mirror-image method is useful for a simple analysis. Figure 2 shows a schematic representation of the mirror images of the electric current sources and sinks (electrical ground) [12]. In this study, the images are for the x- and z-directions.

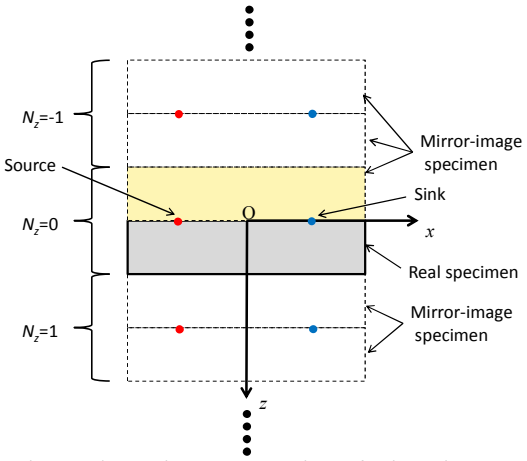

Fig.2 Schematic representation of mirror images.

N_z (half-number of mirror images) denotes the number of sets of plus and minus images in the z-direction. For example, N_z = 0 includes the images from −10 to 10 in the z-direction. If N_z sets of images are required, the electric current density is obtained by summing the electric current densities from the image of #−N_z to that of #N_z: Similarly, N_x denotes the number of sets of plus and minus images in the x-direction, the half number of mirror images. When a specimen is long and the spacing between the source and sink is small enough, the mirror images of the x-direction can be neglected. In this case, the electric

current density is obtained by summing the electric current densities from the images of #$-N_z$ to #N_z (see reference [13]):

$$i_x = \sum_{k=-Nz}^{Nz} \frac{I}{\pi\sqrt{\sigma_x\sigma_z}} \left\{ \frac{x+a}{\frac{(x+a)^2}{\sigma_x}+\frac{(z-2tk)^2}{\sigma_z}} - \frac{x-a}{\frac{(x-a)^2}{\sigma_x}+\frac{(z-2tk)^2}{\sigma_z}} \right\} \tag{7}$$

$$i_z = \sum_{k=-Nz}^{Nz} \frac{I}{\pi\sqrt{\sigma_x\sigma_z}} \left\{ \frac{z-2tk}{\frac{(x+a)^2}{\sigma_x}+\frac{(z-2tk)^2}{\sigma_z}} - \frac{z-2tk}{\frac{(x-a)^2}{\sigma_x}+\frac{(z-2tk)^2}{\sigma_z}} \right\}$$

The appropriate number of images can be determined by comparison of electric current from images. The electric current in the region from $z = 0$ to $z = t$ (the target area of the thin CFRP laminate) of the image is very small when the source-sink couple of an image is located far from the target area. When the source and sink couple is located on the top surface of the specimen, the required number of images can be obtained as follows.

$$N_z \geq 63.7\frac{a\lambda}{2t} \tag{8}$$

The detail of equation (8) is given in reference [13].

Equivalent conductivity of cross-ply laminate

When a beam is composed of 0°-plies and 90°-plies, the simple orthotropic electric potential does not describe the exact electric potential because of the difference between the electrical conductivity of the 0°-plies and 90°-plies [8]. This causes the electric potential difference of a cross-ply laminate to differ from that of a unidirectional CFRP of 0°-plies. To obtain the exact electric current density of a cross-ply laminate, its electric potential difference must be obtained.

In our previous paper [8], it was assumed that the electric potential difference distribution of a cross-ply laminate could be calculated using the electric potential distribution of a uniform orthotropic plate that has a different electrical conductivity from that of the original 0°-ply or 90°-ply. To obtain the electric potential difference distribution of a cross-ply laminate, an equivalent conductance is assumed, which provides it with an almost equal electric potential distribution. When an electric current is applied to the surface of a CFRP plate, the electric potential difference is not uniform in the thickness direction. Figure 3 shows the typical partial difference in the electric potential when the electric source and the sink are placed on the surface of a beam type specimen. This non-uniform electric potential difference requires special measures to the lamination theory of the electrical conductance of CFRP laminates [14].

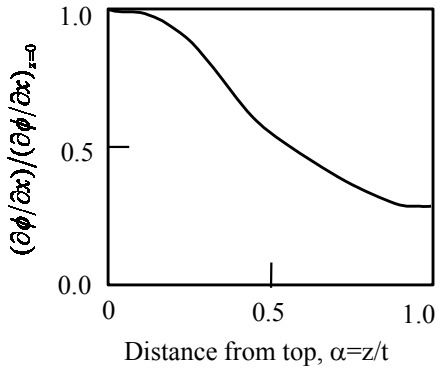

Fig.3 Typical electric potential distribution when electric source and grounding locate on a single surface.

To consider the non-uniform electric potential effect, the previous paper [8] proposed a method that used a contribution function to calculate the equivalent electrical conductance of a cross-ply laminate. The contribution function is the normalized electric potential difference. A small value of the contribution function at normalized depth α (= z/t, where t is the laminate thickness) means that the cross sectional area at thickness α is small for the electric current. Therefore, the width of the area at α is virtually shrunk, and the electrical conductance of the laminate can be calculated.

To obtain the equivalent conductance to allow the electric current density of a cross-ply laminate to be calculated, the following iteration method from reference [8] is available:
(1) Using a unidirectional 0°-ply laminate, the electric potential difference at the center (x = 0) is calculated using the orthotropic electric potential function.
(2) A normalized contribution function $F(\alpha)$ is obtained from the calculated electric potential difference at the M-divided points of the z-coordinate.
(3) Using the obtained contribution function $F(\alpha)$, the equivalent electrical conductance C_x is calculated as follows:

$$C_x = \int_0^1 F(\alpha)\sigma_x d\alpha \tag{9}$$

(4) When the obtained equivalent electrical conductance C_x is different from the previously calculated C_x over the allowable limit value, recalculate the electric potential difference again. When C_x has a small difference compared with the allowable limit value, the iteration is terminated and C_x is assumed to be the equivalent electrical conductance. The full details of the process are given in reference [8].

New theory of anisotropic electric potential function:

Oblique crack analysis

When an electric current source is located at (a_1, t_1) on an infinite plate, the orthotropic electric potential ϕ_s is expressed with small modifications as follows:

$$\phi_s = -\frac{I}{4\pi\sqrt{\sigma_x\sigma_z}}\ln\left\{\frac{(x-a_1)^2}{\sigma_x}+\frac{(z-t_1)^2}{\sigma_z}\right\} \tag{10}$$

When an electrical ground (sink) is located at (a_2, t_2) on the infinite plate, the orthotropic electric potential ϕ_g is expressed as follows:

$$\phi_g = \frac{I}{4\pi\sqrt{\sigma_x\sigma_z}}\ln\left\{\frac{(x-a_2)^2}{\sigma_x}+\frac{(z-t_2)^2}{\sigma_z}\right\} \tag{11}$$

Superposing the source and grounding potential, the orthotropic electric potential function ϕ_d of the oblique electric current (see Fig. 4) in an infinite plate can be obtained as follows:

$$\phi_d = -\frac{I}{4\pi\sqrt{\sigma_x\sigma_z}}\left\{\ln\left(\frac{(x-a_1)^2}{\sigma_x}+\frac{(z-t_1)^2}{\sigma_z}\right)-\ln\left(\frac{(x-a_2)^2}{\sigma_x}+\frac{(z-t_2)^2}{\sigma_z}\right)\right\} \tag{12}$$

Using equation (12), the electric current density can be obtained for the oblique current in the infinite plate.

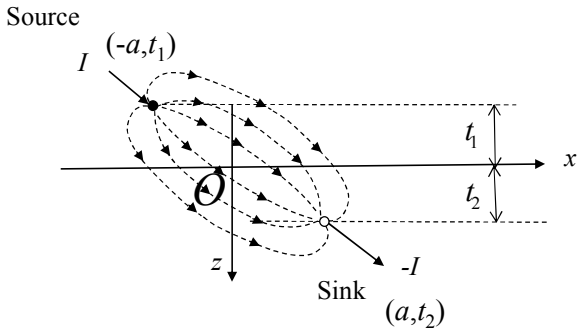

Fig.4 Electric source and ground for oblique electric current in an infinite plate

$$i_x = \frac{I}{\pi\sqrt{\sigma_x\sigma_z}}\left\{\frac{x-a_1}{\frac{(x-a_1)^2}{\sigma_x}+\frac{(z-t_1)^2}{\sigma_z}} - \frac{x-a_2}{\frac{(x-a_2)^2}{\sigma_x}+\frac{(z-t_2)^2}{\sigma_z}}\right\} \tag{13}$$

$$i_z = \frac{I}{\pi\sqrt{\sigma_x\sigma_z}}\left\{\frac{z-t_1}{\frac{(x-a_1)^2}{\sigma_x}+\frac{(z-t_1)^2}{\sigma_z}} - \frac{z-t_2}{\frac{(x-a_2)^2}{\sigma_x}+\frac{(z-t_2)^2}{\sigma_z}}\right\}$$

When the analytical results are compared with experimental results, the dot-like electrodes are not realistic. The orthotropic electric potential function for finite-width electrodes ϕ_L can be obtained by integrating the electric potential function of dot-like electrodes given by equation (12) along the electrode lines. Let us consider the case that the electrodes have finite length as shown in Fig. 5. The integrated potential function for the line electrode ϕ_L is given as follows:

$$\varphi_L = \int_{-b_2}^{-b_1} \varphi_s dl_1 + \int_{b_1}^{b_2} \varphi_g dl_2 \tag{14}$$

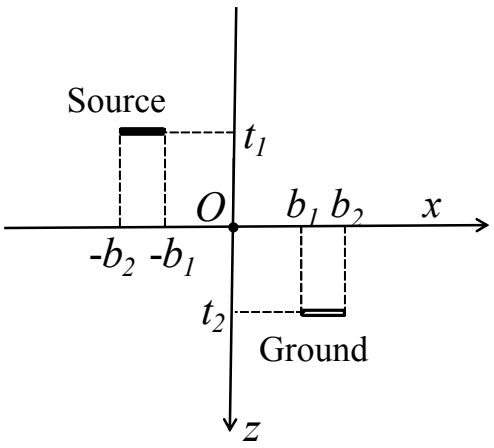

Fig.5 Line source and line ground for oblique electric current in an infinite plate.

The electric current density can be calculated as follows

$$i_x = -\sigma_x \frac{\partial \varphi_L}{\partial x} \tag{15}$$

$$i_z = -\sigma_z \frac{\partial \varphi_L}{\partial z} \tag{16}$$

The effect of the specimen thickness cannot be neglected for the oblique electric current because the electric current flows in the through-thickness direction from the top surface to the bottom surface (see Fig. 6). The thickness effect can be modified using the mirror image method. The mirror image of the oblique electric current is illustrated in Fig. 7. The mirror images in the z-direction must be placed for the oblique electric current. Because the 0th mirror image exists, the total source electric current must be 2I to apply an electric current of I in the actual CFRP beam.

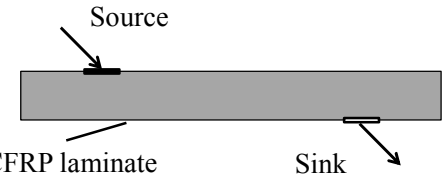

Fig.6 Oblique electric current specimen of beam type.

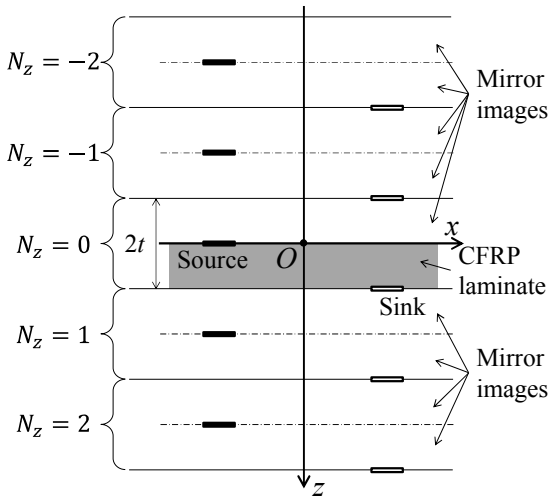

Fig.7 Mirror images of z-direction for oblique electric current

The total number of mirror images in the z-direction, N_z, for the approximations is determined from the electric current of the mirror image compared with the total electric current applied in the target specimen.

The electric current density of the original source and sink at the middle of the beam ($x = 0$) can be obtained from equation (16) when $2I$ is applied as follows:

$$i_x\big|_{x=0} = -\sigma_x \left.\frac{\partial \varphi_L}{\partial x}\right|_{x=0} \tag{17}$$

Let us consider that the half number of mirror images is set to N_z. This means that the N_z mirror images are located in the upper half of the original specimen, and the same number of images is located in the lower half of the original specimen. Thus, a total of ($2N_z + 1$) source and sink couples exist aligned in z-direction

When the spacing between the electrodes is not small enough compared with the specimen length, the *x*-direction mirror images must be added as shown in Fig. 8. Let the half number of mirror images in the x-direction equal $2N_x$. Because the distance to the source from the center of the specimen is b_1, the electric current density from the mirror image of the *k*th location can be calculated by replacing *x* with $x-kL$ when *k* is an even number. When *k* is an odd number, the source and sink exchange their position as shown in Fig. 8.

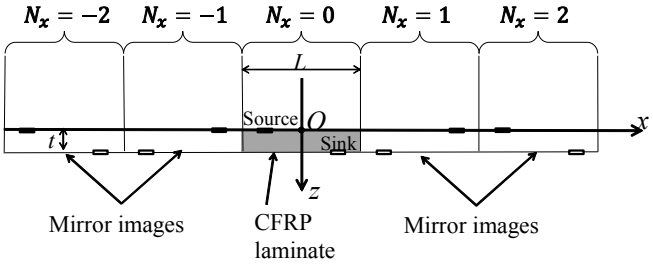

Fig.8 Mirror images of *x*-direction for oblique electric current

Analysis of laminated CFRP plate

The electric conductivities in the *x*-, *y*- and *z*-directions are σ_x, σ_y and σ_z respectively. The electric current density in each direction can be expressed as follows,

$$i_x = -\sigma_x \frac{\partial \phi}{\partial x}, \quad i_x = -\sigma_y \frac{\partial \phi}{\partial y} \quad , \quad i_z = -\sigma_z \frac{\partial \phi}{\partial z} \tag{18}$$

The continuity of electric current gives the following equation,

$$\sigma_x \frac{\partial^2 \phi}{\partial x^2} + \sigma_y \frac{\partial^2 \phi}{\partial y^2} + \sigma_z \frac{\partial^2 \phi}{\partial z^2} = 0 \tag{19}$$

Affine transformations are adopted as follows,

$$\xi = \frac{x}{\sqrt{\sigma_x}}, \ \eta = \frac{y}{\sqrt{\sigma_y}}, \ \zeta = \frac{z}{\sqrt{\sigma_z}} \tag{20}$$

Using the affine transformation, equation (2) becomes,

$$\frac{\partial^2 \phi}{\partial \xi^2} + \frac{\partial^2 \phi}{\partial \eta^2} + \frac{\partial^2 \phi}{\partial \zeta^2} = 0 \tag{21}$$

Similar to the two dimensional analysis, electric potential function of 3D plate is obtained as follows [8].

$$\phi_{source} = \frac{I}{2\pi\sqrt{\sigma_x \sigma_y \sigma_z}} \frac{1}{\sqrt{\frac{(x-a_{1x})^2}{\sigma_x} + \frac{(y-a_{1y})^2}{\sigma_y} + \frac{z^2}{\sigma_y}}} \tag{22}$$

$$\phi_{sink} = -\frac{I}{2\pi\sqrt{\sigma_x \sigma_y \sigma_z}} \frac{1}{\sqrt{\frac{(x-a_{2x})^2}{\sigma_x} + \frac{(y-a_{2y})^2}{\sigma_y} + \frac{z^2}{\sigma_y}}} \tag{23}$$

For damage monitoring using changes in electrical resistance, the electrodes are not a single point, but rectangular as shown in Fig.9. To obtain the electric potential of finite area electrodes, the electric potential function is integrated over the electrode area as shown in the equation (24).

$$\phi = \frac{1}{2a_y(a_{2x}-a_{1x})}\left(\int_{-a_y}^{a_y}\int_{-a_{2x}}^{-a_{1x}}\phi_{source}da_{1x}da_{1y} + \int_{-a_y}^{a_y}\int_{a_{1x}}^{a_{2x}}\phi_{sink}da_{2x}da_{2y}\right) \tag{24}$$

The electric potential function shown in the equation (24) is applicable for an infinite body. For a finite plate, the electric potential function can be modified using mirror images.

Let us think about the situation in which electric current source forms a line (Fig. 9). This situation corresponds to the electrode arrangements employed as Addressable Conducting Network (ACN) for self-sensing of damage in CFRP structure [10]. When the electric current source is a line, the line can be considered as the set of source points. Electric potential function for source point located at (-a, a_y, 0) ϕ_{point} can be expressed as

$$\phi_{\text{point}} = \frac{I}{4\pi(a_{2y}-a_{1y})\sqrt{\sigma_x\sigma_y\sigma_z}}\frac{1}{\left(\frac{(x+a)^2}{\sqrt{\sigma_x}}+\frac{(y-a_y)^2}{\sqrt{\sigma_y}}+\frac{z^2}{\sqrt{\sigma_z}}\right)^{1/2}} \tag{25}$$

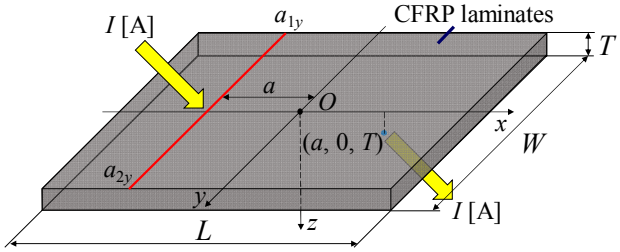

Fig. 9. Unidirectional CFRP laminate with electric current source line and sink point.

Integrating this function over the line ($a_{1y} \le$ y $\le$ a_{2y}), the electric potential function for the line source ϕ_{line} can be obtained as

$$\phi_{\text{line}} = \int_{a_{1y}}^{a_{2y}}\phi_{\text{point}}da_y = \frac{I}{4\pi(a_{2y}-a_{1y})\sqrt{\sigma_x\sigma_z}}\ln\frac{\sqrt{\frac{(x+a)^2}{\sigma_x}+\frac{(y-a_{2y})^2}{\sigma_y}+\frac{z^2}{\sigma_z}}-\frac{y-a_{2y}}{\sqrt{\sigma_y}}}{\sqrt{\frac{(x+a)^2}{\sigma_x}+\frac{(y-a_{1y})^2}{\sigma_y}+\frac{z^2}{\sigma_z}}-\frac{y-a_{1y}}{\sqrt{\sigma_y}}} \tag{26}$$

The orthotropic electric potential function ϕ for a couple of source line and sink point described in Fig. 9 can be expressed as

$$\phi = \frac{I}{4\pi\sqrt{\sigma_x\sigma_y\sigma_z}}\left\{\frac{\sqrt{\sigma_y}}{(a_{2y}-a_{1y})}\ln\frac{\sqrt{\frac{(x+a)^2}{\sigma_x}+\frac{(y-a_{2y})^2}{\sigma_y}+\frac{z^2}{\sigma_z}}-\frac{y-a_{2y}}{\sqrt{\sigma_y}}}{\sqrt{\frac{(x+a)^2}{\sigma_x}+\frac{(y-a_{1y})^2}{\sigma_y}+\frac{z^2}{\sigma_z}}-\frac{y-a_{1y}}{\sqrt{\sigma_y}}}-\frac{1}{\left(\frac{(x-a)^2}{\sqrt{\sigma_x}}+\frac{y^2}{\sqrt{\sigma_y}}+\frac{z^2}{\sqrt{\sigma_z}}\right)^{1/2}}\right\} \tag{27}$$

When an electric current source and a ground are located on the top surface of a laminated CFRP plate, the electric potential difference has its maximum value at the surface, and decreases with increasing distance from the surface. The decrease of the electric potential difference arises from the low electrical conductivity in the though-thickness direction. The distribution of the electrical potential depends on the ratio of electrical conductivity between σ_x and σ_z. For cross-ply laminates, σ_x gives the exact distribution of the electric potential, and the electric potential difference is not equal to σ_0 or σ_{90}. The modified process used two directions, and is described briefly as follows.

(1) Using a unidirectional 0°-ply laminate, the electric potential differences ($\partial\phi/\partial x$ and $\partial\phi/\partial y$) at one point (x, y) = ($-a_{1x}$, a_{1x}) are calculated using the orthotropic electric potential function. Note that the point should not be on the coordinate axis (x=0 and y=0).

(2) Normalized contribution functions $F_x(\alpha)$ and $F_y(\alpha)$ are obtained from the calculated electric potential difference ($\alpha = z/t$: where t is the plate thickness).
(3) Using the obtained contribution functions $F_x(\alpha)$ and $F_y(\alpha)$, the equivalent electrical conductivities C_x and C_y are calculated as follows

$$C_x = \int_0^t F_x(\alpha)\sigma_x d\alpha\,,\quad C_y = \int_0^t F_y(\alpha)\sigma_y d\alpha \tag{28}$$

(4) When the obtained equivalent electrical conductivities C_x and C_y are different from the previously calculated C_x and C_y, and above a certain allowable limit, the electric potential difference is recalculated. When C_x has a small difference relative to its allowable limit, the iteration is terminated and C_x is assumed to be equivalent to the electrical conductance. Using the equivalent conductivities C_x and C_y, the electric potential function of the laminated plate is obtained.

Let us consider a case in which the fiber direction is rotated by θ from the x-axis as shown in Fig. 10. The electric current can be calculated as follows

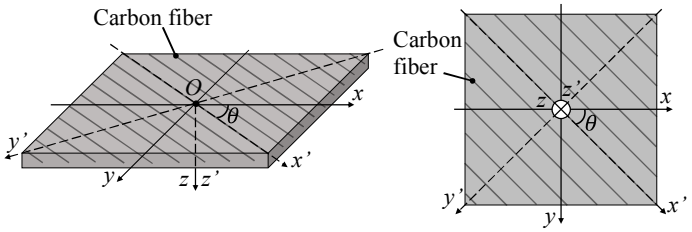

Fig.10 Definition of fiber rotation angle and x-y coordinates.

$$\begin{bmatrix} i_x \\ i_y \\ i_z \end{bmatrix} = -\begin{bmatrix} \sigma_{xx} & \sigma_{xy} & 0 \\ \sigma_{xy} & \sigma_{yy} & 0 \\ 0 & 0 & \sigma_t \end{bmatrix} \begin{bmatrix} \dfrac{\partial \phi}{\partial x} \\ \dfrac{\partial \phi}{\partial y} \\ \dfrac{\partial \phi}{\partial z} \end{bmatrix} \tag{29}$$

$$\begin{aligned} \sigma_{xx} &= \sigma_0 \cos^2\theta + \sigma_{90}\sin^2\theta \\ \sigma_{xy} &= (\sigma_0 - \sigma_{90})\sin\theta\cos\theta \\ \sigma_{yy} &= \sigma_0 \sin^2\theta + \sigma_{90}\cos^2\theta \end{aligned} \tag{30}$$

When θ = 0° or θ = 90°, σ_{xy} in the equation (30) becomes zero. For the angle plies, σ_{xy} is non-zero. A non-zero σ_{xy} transforms the equation for the continuity of electric current into a non-Laplace equation. The non-Laplace equation means that the orthotropic electric potential function cannot be applied when the angle plies are included in the laminated CFRP plate. In the present study, therefore, a new approximation method is proposed.

To prevent bending-twisting coupling, angle plies are usually placed adjacent. For example, 45° and −45°-plies are placed adjacent in most real laminated CFRP plates. Even when another ply such as a 90°-ply is included, the 90°-ply is sandwiched between the 45°-ply and −45°-ply to prevent bending-twisting coupling. In the present study, two cases are considered: first, where 45° and −45°-plies are adjacent, and the second, where the layers are arranged in the order 45°-ply, 90°-ply and −45°-ply. Placement of a 0°-ply instead of a 90°-ply, can be considered by replacing the 90°-ply with the 0°-ply.

When a 45°-ply and −45°-ply are adjacent, the two layers can be coupled and assumed to be a ply of double thickness (±45°-ply) as shown in Fig. 11(a). The coupling of the plies makes the overall value of $\sigma_{xy} = 0$, from equation (9). This means that the double thickness ±45°-ply can be treated as an orthotropic ply of conductivity of (σ_0 + σ_{90})/2. The orthotropic potential function can then be obtained using the equivalent conductivity analysis shown in previous section. The equivalent

conductivity of the laminated CFRP enables us to calculate the electric potential difference, and the electrical current density for each angle ply using equation (29). For example, the 45°-ply has σ_{xy} of $(\sigma_0 - \sigma_{90})/2$. The coupling of the ±45°-plies used in the electric potential function is a smooth continuous function and the function of 45°-ply or −45°-ply can be approximated by ±45°-ply.

When a 90°-ply is located between the ±45°-plies, the three plies (45°-ply, 90°-ply and −45°-ply) couple to other cases of ±45°-plies. The thickness of the coupled ply is three times that of a normal ply, as shown in Fig. 11 (b). The triple-ply coupling makes σ_{xy} zero. This coupling also enables us to calculate the orthotropic electric potential function for a laminate that includes angle plies. The triple thickness ply has $\sigma_x = (\sigma_0+2\sigma_{90})/3$ and $\sigma_y = (2\sigma_0+\sigma_{90})/3$. This enables us to calculate the equivalent conductivity. The equivalent conductivity gives the electric potential function, and the electric current density can be obtained using equation (29).

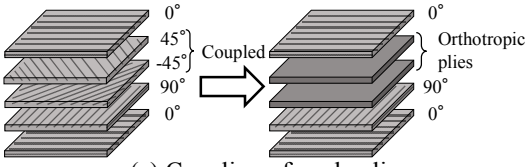

(a) Coupling of angle plies.

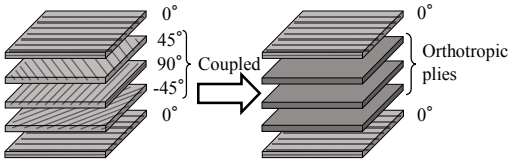

(b) Coupling of angle plies with other ply

Fig.11 Schematic representation of coupled laminates used to calculate equivalent conductivity

Delamination analysis

Delamination cracks are treated as zero-thickness planes that act as insulating material in regard to electric current flowing in the through-thickness direction. The electric current field of the laminates with delamination can be expressed as a superposition of two components: the first is the field induced by the electric current source and sink, and the second is the field induced by the sets of doublets introduced on the delamination surfaces to annul the electric current flow in the through-thickness direction. The details of this doublet analysis method are stated as follows.

A three-dimensional Cartesian coordinate system is introduced. When a doublet of strength μ directed along the z direction is located at (x_0, y_0, dz), the electric potential, ϕ_{doublet}, at field point (x, y, z) due to the doublet can be expressed as [12] [13]

$$\phi_{doublet} = \frac{\mu(x_0, y_0, d_z)}{4\pi} \frac{\dfrac{z-d_z}{\sqrt{\sigma_z}}}{\left\{\dfrac{(x-x_0)^2}{\sigma_x} + \dfrac{(y-y_0)^2}{\sigma_y} + \dfrac{(z-d_z)^2}{\sigma_z}\right\}^{\frac{3}{2}}} \tag{31}$$

Using Ohm's law, the electric current density, $i_{z,\text{ doublet}}$, in the z direction induced by the doublet at (x_0, y_0, dz) can be expressed as

$$i_{z,doublet}(x,y,z) = \mu(x_0, y_0, d_z)\frac{\sqrt{\sigma_z}}{4\pi} \frac{\dfrac{(x-x_0)^2}{\sigma_x} + \dfrac{(y-y_0)^2}{\sigma_y} - 2\dfrac{(z-d_z)^2}{\sigma_z}}{\left\{\dfrac{(x-x_0)^2}{\sigma_x} + \dfrac{(y-y_0)^2}{\sigma_y} + \dfrac{(z-d_z)^2}{\sigma_z}\right\}^{\frac{5}{2}}} \tag{32}$$

Doublets are introduced over the entire delamination area. The electric current density, $i_{z,\,crack}$, in the z direction at point (x, y, z) induced by all the doublets can be calculated from the surface integral,

$$i_{z,crack}(x,y,z)=\frac{\sqrt{\sigma_z}}{4\pi}\iint\mu(x_0,y_0,d_z)\frac{\dfrac{(x-x_0)^2}{\sigma_x}+\dfrac{(y-y_0)^2}{\sigma_y}-2\dfrac{(z-d_z)^2}{\sigma_z}}{\left\{\dfrac{(x-x_0)^2}{\sigma_x}+\dfrac{(y-y_0)^2}{\sigma_y}+\dfrac{(z-d_z)^2}{\sigma_z}\right\}^{\frac{5}{2}}}dx_0dy_0 \tag{33}$$

The domain of integration is the surface area affected by delamination. Let us assume that the electric current source and sink are present in the field. As the electric current density on the delamination surface needs to be zero in the direction perpendicular to this surface, then the equation for equilibrium

$$i_z(x,y,z)+i_{z,crack}(x,y,z)=0 \tag{34}$$

must hold on the delamination surface. Here, i_z is electric current density induced by the current source and sink. This situation is depicted in Fig. 12 Equation (34) gives the strength of the doublet μ, which leads to the change in the electric potential caused through delamination given by Equation (31). Solving Equation (34), however, is difficult because Equation (33) is a hyper-singular integral equation evaluated over the delamination surface; $z = dz$. A method of approximation to obtain μ is therefore proposed that avoids the singularity by considering the equation of equilibrium at a point slightly shifted from the delamination surface; $z = dz$ - ε. Here, ε is a small nonzero value. To calculate μ, the delamination surface is divided into $M_x \times M_y$ grids (Fig. 13). Throughout the grid, μ is assumed to be constant equal to its value at the center of the grid (x_m, y_l, dz). This discretization technique enables Equation (34) to be written as

$$i_z(x,y,z)=-\frac{\sqrt{\sigma_z}}{4\pi}\sum_{m=1}^{N_x}\sum_{l=1}^{N_y}\mu_{ml}\frac{\dfrac{(x-x_m)^2}{\sigma_x}+\dfrac{(y-y_l)^2}{\sigma_y}-2\dfrac{(z-d_z)^2}{\sigma_z}}{\left\{\dfrac{(x-x_m)^2}{\sigma_x}+\dfrac{(y-y_l)^2}{\sigma_y}+\dfrac{(z-d_z)^2}{\sigma_z}\right\}^{\frac{5}{2}}}\Delta S \tag{35}$$

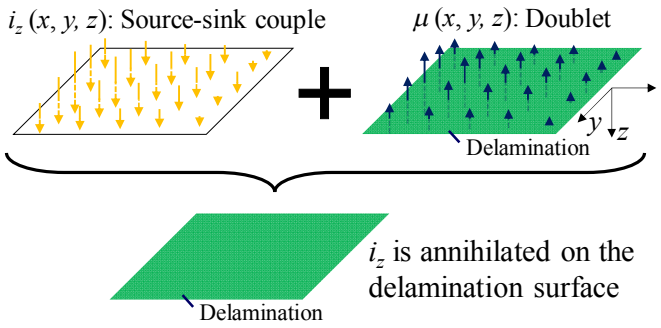

Fig.12 Principle of superposition of doublets on the delamination surface.

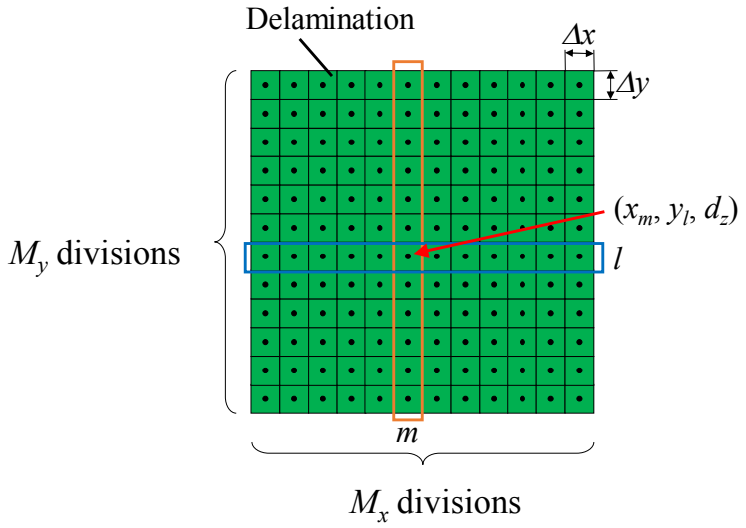

Fig.13 Grid divisions of delamination surface for the surface integral calculation.

Here, μ_{ml} is defined as the value of the strength at (x_m, y_l, dz), and ΔS is the product $\Delta x\ \Delta y$; x_s and y_r are defined similar to x_m, y_l, i.e., the x and y coordinates at the center of the grid. In addition, i_{sr} and F_{srml} are defined as

$$i_{sr} = i_z(x_s, y_r, d_z - \varepsilon) = -\frac{\sqrt{\sigma_z}}{4\pi}\sum_{m=1}^{N_x}\sum_{l=1}^{N_y}\mu_{ml}\frac{\dfrac{(x_s-x_m)^2}{\sigma_x}+\dfrac{(y_r-y_l)^2}{\sigma_y}-2\dfrac{\varepsilon^2}{\sigma_z}}{\left\{\dfrac{(x_s-x_m)^2}{\sigma_x}+\dfrac{(y_r-y_l)^2}{\sigma_y}+\dfrac{\varepsilon^2}{\sigma_z}\right\}^{\frac{5}{2}}}\Delta S \tag{36}$$

$$F_{srml} = -\frac{\sqrt{\sigma_z}}{4\pi}\frac{\dfrac{(x_s-x_m)^2}{\sigma_x}+\dfrac{(y_r-y_l)^2}{\sigma_y}-2\dfrac{\varepsilon^2}{\sigma_z}}{\left\{\dfrac{(x_s-x_m)^2}{\sigma_x}+\dfrac{(y_r-y_l)^2}{\sigma_y}+\dfrac{\varepsilon^2}{\sigma_z}\right\}^{\frac{5}{2}}}\Delta S \tag{37}$$

Using i_{sr} and F_{srml}, Equation (35) can be written as

$$i_{sr} = F_{srml}\mu_{ml} \tag{38}$$

$$[i] = [i_{11}\cdots i_{M_x1}\, i_{12}\cdots i_{M_x2}\ \cdots i_{1M_y}\cdots i_{M_xM_y}]^T \tag{39}$$

$$[F]=\begin{bmatrix} F_{1111} & \cdots & F_{11M_x1} & F_{1112} & \cdots & F_{11M_x2} & \cdots & F_{111M_y} & \cdots & F_{11M_xM_y} \\ \vdots & \ddots & \vdots & \vdots & \ddots & \vdots & \ddots & \vdots & \ddots & \vdots \\ F_{M_x111} & \cdots & F_{M_x1M_x1} & F_{M_x112} & \cdots & F_{M_x1M_x2} & \cdots & F_{M_x11M_y} & \cdots & F_{M_x1M_xM_y} \\ F_{1211} & \cdots & F_{12M_x1} & F_{1212} & \cdots & F_{12M_x2} & \cdots & F_{121M_y} & \cdots & F_{12M_xM_y} \\ \vdots & \ddots & \vdots & \vdots & \ddots & \vdots & \ddots & \vdots & \ddots & \vdots \\ F_{M_x211} & \cdots & F_{M_x2M_x1} & F_{M_x212} & \cdots & F_{M_x2M_x2} & \cdots & F_{M_x21M_y} & \cdots & F_{M_x2M_xM_y} \\ \vdots & \ddots & \vdots & \vdots & \ddots & \vdots & \ddots & \vdots & \ddots & \vdots \\ F_{1M_y11} & \cdots & F_{1M_yM_x1} & F_{1M_y12} & \cdots & F_{1M_yM_x2} & \cdots & F_{1M_y1M_y} & \cdots & F_{1M_yM_xM_y} \\ \vdots & \ddots & \vdots & \vdots & \ddots & \vdots & \ddots & \vdots & \ddots & \vdots \\ F_{M_xM_y11} & \cdots & F_{M_xM_yM_x1} & F_{M_xM_y12} & \cdots & F_{M_xM_yM_x2} & \cdots & F_{M_xM_y1M_y} & \cdots & F_{M_xM_yM_xM_y} \end{bmatrix} \tag{40}$$

$$[\mu]=[\mu_{11}\cdots\mu_{M_x1}\,\mu_{12}\cdots\mu_{M_x2}\;\cdots\mu_{1M_y}\cdots\mu_{M_xM_y}]^T \tag{41}$$

Their relationship is expressible as

$$[\mathbf{i}]=[\mathbf{F}][\boldsymbol{\mu}] \tag{42}$$

Multiplying both sides of Equation (42) from the left with the inverse matrix of [F], $[F]^{-1}$, one obtains

$$[\boldsymbol{\mu}]=[\boldsymbol{F}]^{-1}[\boldsymbol{i}] \tag{43}$$

Using each component of [μ] gives the change in electric potential induced by each doublet introduced on the delamination surface. This change in electric potential induced by delamination cracks can be obtained from the integrals of all contributions from the entire set of doublets. The change in electric potential at (x, y, z), ϕ_{crack}, therefore, is calculated using Equation (31) and values obtained for μ_{ml},

$$\phi_{crack}(x,y,z)=-\frac{1}{4\pi}\sum_{m=1}^{N_x}\sum_{l=1}^{N_y}\mu_{ml}\frac{\dfrac{z-d_z}{\sqrt{\sigma_z}}}{\left\{\dfrac{(x-x_m)^2}{\sigma_x}+\dfrac{(y-y_l)^2}{\sigma_y}+\dfrac{(z-d_z)^2}{\sigma_z}\right\}^{\frac{3}{2}}}\Delta S \tag{44}$$

For an accurate solution, the contribution from the sets of image charge doublets surrounding the object also needs to be superposed. Calculating the strengths of all doublets, however, takes a long time. The doublet-analysis method has the advantage in providing a less intensive calculation compared with commonly-used numerical methods such as FEM. In the present study, the set of doublets from only one image charge adjacent to the object in the through-thickness direction is superposed to affect a low calculation cost. Considering this image charge, the change in the electric potential ΔV on the top surface (x, y, 0) induced by delamination cracks can be expressed as

$$\Delta V=2\phi_{crack}(x,y,0)=\frac{1}{2\pi}\sum_{m=1}^{N_x}\sum_{l=1}^{N_y}\mu_{ml}\frac{\dfrac{d_z}{\sqrt{\sigma_z}}}{\left\{\dfrac{(x-x_m)^2}{\sigma_x}+\dfrac{(y-y_l)^2}{\sigma_y}+\dfrac{d_z^{\,2}}{\sigma_z}\right\}^{\frac{3}{2}}}\Delta S \tag{45}$$

Experiments and FEM analyses:
Oblique current beam type
(a) FEM analysis

The results of the new analysis method of the oblique electric current are compared with the results of FEM analysis. Because the FEM analysis is based on the assumption that the laminated composites can be dealt with as homogeneous orthotropic conductive materials, success does not mean that the result given by the new analysis method is exactly equal to the actual electric current. If the analysis results agree with the FEM results, it simply means that the calculation of the equivalent conductivity of the laminated composites is effective for the applied oblique electric current.

ANSYS Mechanical APDL ver.15.0 was used for the FEM analysis. Type PLANE 230 (4-Node quadrilateral plane) elements were adopted for the analysis. The specimen configuration is shown in Fig. 14. The beam type specimen was divided into 102400 meshes. The typical mesh size was 0.5 mm in the specimen length direction and 0.019 mm in the thickness direction. At the electrodes, copper elements were attached, 50 mA was applied to the electric source electrode, and the voltage was set to 0 V at the grounding electrode. The specimen length was 640 mm and the thickness was 1.52 mm. Two types of stacking sequences were computed: unidirectional $[0_8]_T$ and cross-ply $[(0/90)_2]_S$. The electric conductivity used for the FEM analysis and the oblique flow potential analysis method from reference [9] is shown in Table 1.

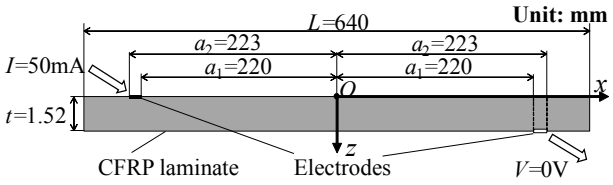

Fig.14 Specimen configuration used for FEM analysis

Table 1 Electric conductivity used for FEM analysis [9].

Fiber direction	Transverse direction	Through the thickness direction	
		UD	Cross-ply $[(0/90)_2]_S$
4.93×10^{4}	6.54	3.63×10^{-3}	7.25×10^{-2}

(b) Experimental comparisons

The comparison with the FEM results does not reveal the effectiveness of the assumption that the laminated composites with resin rich layers can be treated as an orthotropic homogeneous material for an electric current in the through-thickness direction. For confirmation, an experimental process is indispensable. In the present section, an oblique electric current experimentally applied to the two types of specimens, unidirectional and cross-ply laminated beam specimens, is investigated. The electric current was experimentally measured and compared with the results of the oblique flow potential analysis method.

To measure the electric current flows in each ply, special specimens that had separated plies at the middle were fabricated as shown in Fig. 15. At the middle of the specimen, pairs of plies were coupled together to prevent failure of the plies during the curing process, and the coupled plies were electrically separated from other coupled plies using polytetrafluoroethylene film. The beam type specimen was divided into two parts at the middle. At the separated middle edges, copper electrodes were made on every ply couple using the copper plating method. To measure the electric current in each coupled layer, the specimens were connected through corresponding plies with lead wires, as shown in Fig. 15. The current flowing in each ply converged on the center lead wire. Therefore, the amount of current flowing in each ply could be measured by measuring the current flowing in each lead wire. To measure the electric current, noncontact-current-Hall-effect sensors (MCS-SD2537: GRID Inc., HDCC-30mA-D1, HDCC-3mA-D1: Hohkohsya, Tokyo, Japan) were attached to the lead wires. Current sensors

based on the Hall-effect do not affect the current distribution in a specimen. The current sensors were connected to an oscilloscope (Picoscope4424: Pico Technology, Tokyo, Japan), and DC source power supply equipment (PW18-1.3AT: Kenwood, Tokyo, Japan) was used to input 50 mA current.

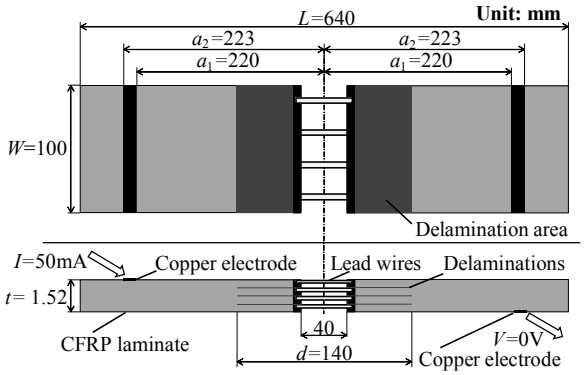

Fig.15 Configuration of specimen with separated area in the center
of the specimen used for experimental measurement of electric current.

Electrical conductivity was measured with an LCR meter (LCR Hitester 3522: Hioki E. E. Corporation, Tokyo, Japan) using direct current [9].

In the present study, two types of stacking sequences of beam-type laminates were prepared: unidirectional CFRP $[0]_8$ and cross-ply CFRP $[(0/90)_2]_S$. The electric conductivity in the fiber, transverse, and thickness directions that were required to be analyzed were measured using an actual CFRP specimen (T800S/3900-2B, P2352W-19: Toray Industries Inc., Tokyo, Japan).

Plate current type

The electric current density results of three types of laminates were calculated using the new method and compared with computational results obtained using Finite Difference Method (FDM) to confirm the performance of the new method. The laminated CFRP plate model is shown in Figure 16. The dimensions of the plate were 40 mm × 40 mm × 1 mm. For analysis of the electrical current, only the ratio of electric conductivity is important. The electric conductivities in the analysis, therefore, are $\sigma_0 = 1$, $\sigma_{90} = 0.1$ and $\sigma_t = 0.01$. An electric current is applied to an electrode with an area of 0.8×0.8 mm^2. A grounding electrode also had a similar area. The spacing between the electrodes was set to 20 mm. The applied electric current I was 1000 mA. Three types of laminates were modeled: unidirectional $[0_{10}]_T$, $[0/45/-45/90/0]_S$ and $[0/45/90/-45/0]_S$.

FDM was used for the computational analysis in the present study. The grid spacing in the x and y direction was set to 0.2 mm and that in the z direction was set to 0.02 mm. The total number of grids was 2,000,000. To check for convergence of computation iterations, the total electric current in the x direction at the cross section of $y = 0$ was compared with the applied electric current I. For the iteration computations, super parallel computing CUDA ver. 7.0 was performed using a GeForce GTX 970 made by NVIDIA to reduce the computational cost. The total computing time for the analysis was approximately 120 hours. Comparisons were performed at the origin $(x, y) = (0, 0)$ of the plate shown in Figure 16 and at a point A $(x, y) = (-5, 5)$. Because there is no electric current in the y direction at the origin, the electric current density in the x direction was compared with the results of the new analysis at the origin. At point A, the electric currents in the x and y directions were compared with the results of the new analysis.

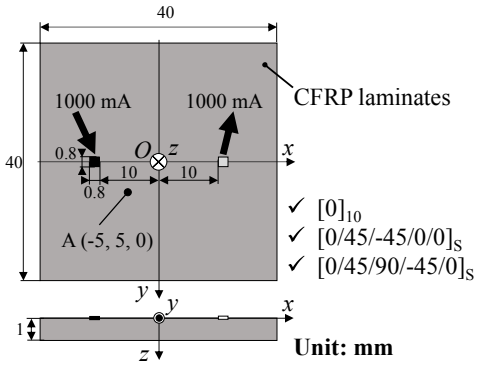

Fig.16 Configuration of a CFRP plate used for analysis.

Delamination analysis

Three different models are studied: the first has one large delamination, the second has two small delaminations and the third has one small delamination, named as model 1, model 2 and model 3 respectively. Details of the model dimensions are illustrated in Fig. 17. The fiber is directed along the x direction (unidirectional). The input electric current I is set to 1 A; the distance between the current input/output area and the origin is set at 10 mm. The important parameters for electrical analysis are the ratios of electrical conductivity for each direction; the electric conductivities for the three directions are set to $\sigma_x = 1$ S/m, $\sigma_y = 0.1$ S/m and $\sigma_z = 0.01$ S/m. The dimensions of the delamination are set to 6 mm × 6 mm for model 1, and 4 mm × 4 mm for model 2 and model 3. The centers of the delaminations are located at $(d_x, d_y, d_z) = (-6, 0, 0.1)$ for model 1, at $(-10, 0, 0.4)$ and $(2, 0, 0.1)$ for model 2 and at $(-5, 5, 0.1)$ for model 3. For the FEM analysis, rectangular elements having dimensions of 0.5 mm × 0.5 mm × 0.025 mm were adopted. Nodes on the delamination surface are doubly defined and not merged, hence blocking any electrical conduction in the through-thickness direction. In the doublet-analysis method, the short distance ε in Equations (36) and (37) is set to 0.01 mm to avoid the singularity in the equilibrium equation. Discretization was done by dividing the delamination area into 21 × 21 grids for model 1, and 14 × 14 grids for model 2 and model 3. The change in electric potential on the top surface, i.e., z = 0, was calculated by the doublet-analysis method and FEM, and compared for both cases.

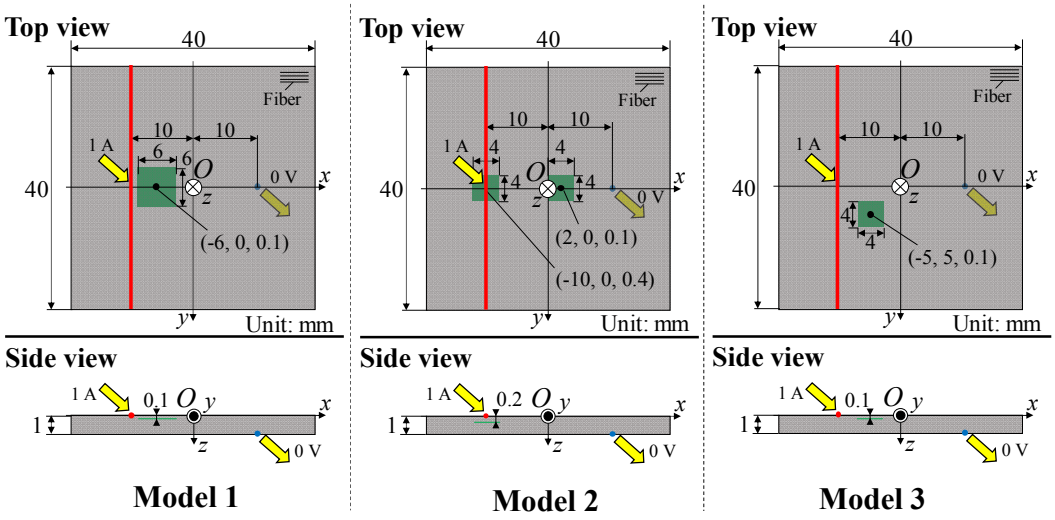

Fig.17 Schematic representations of three different kinds of the analytical models with delamination cracks.

Results and Discussion:

Oblique current beam type

(a) FEM analysis

Figure 18 shows the electric current density in the x-direction at $x = -100$ mm of the unidirectional specimen. The abscissa is the distance from the upper surface and the ordinate is the electric current density. Even at the $x = 100$ mm location, the electric current density obtained using the oblique flow potential analysis agree well with the results of the FEM analysis for this unidirectional specimen.

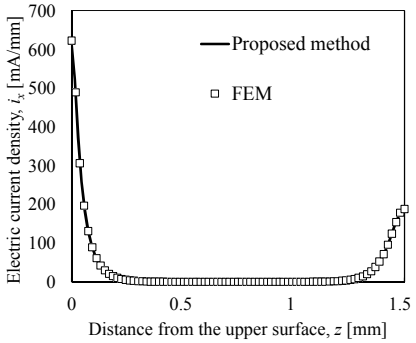

Fig.18 Comparison of electric current density ix of unidirectional laminate specimen at x=-100 mm

Figure 19 shows the electric current density in the x-direction at the center of the ($x = 0$) of the cross-ply laminate specimen. For this specimen, the oblique flow potential analysis requires an equivalent conductivity in the x-direction to represent the electric voltage distribution of the cross-ply laminated specimen, which is treated as a homogeneous material with the same electric voltage difference distribution. In the present study, the equivalent conductivity in the x-direction was $C_x = 2.94 \times 10^4$ S/m. The obtained equivalent conductivity C_x and the new orthotropic electric potential analysis method can be used to determine the electric voltage distribution. For the calculations with the new analysis method, the total number of mirror images in the thickness direction is $N_z = 6$, and the total number of mirror images in the x-direction is $N_x = 48$. The electric current density can be calculated from the obtained electric voltage difference. The calculated results are shown in Fig. 19 as rectangular symbols.

Figure 18 and 19 show that the electric current density calculated by the oblique flow potential analysis method almost completely agrees with the FEM results.

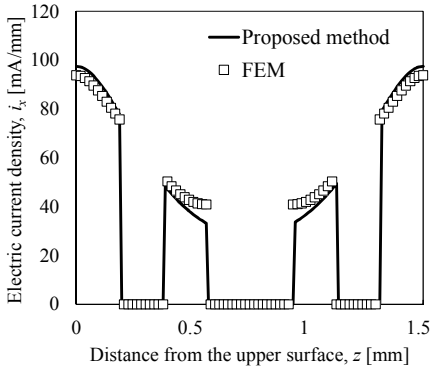

Fig.19 Comparison of electric current density i_x of cross-ply laminate specimen at x=0 mm.

(b) Experimental comparisons

Figure 20 shows a comparison of the experimental results with the results of the oblique flow potential analysis method for the unidirectional specimen. Figure 21 shows the comparison of the results of experiments with the results of the oblique flow potential analysis method of the cross-ply specimen. The abscissa shows the coupled layer number and the ordinate

shows the electric current. The coupled layers are numbered from the upper coupled plies; layer number 1 is the upper layer and layer number 4 is the bottom layer. The electric current means the total sum of the electric current flows in the two coupled piles. The results of the oblique flow potential analysis method, therefore, are the integrated results in the two coupled plies.

The open squares represent the measured experimental results and the solid circles represent the results of the oblique flow potential analysis method. The results of the oblique flow potential analysis method agree well with the measured electric current. This means that the assumption of an orthotropic homogeneous material is effective even for oblique electric current in toughened laminated composites: the thick resin rich layer is negligible for analysis.

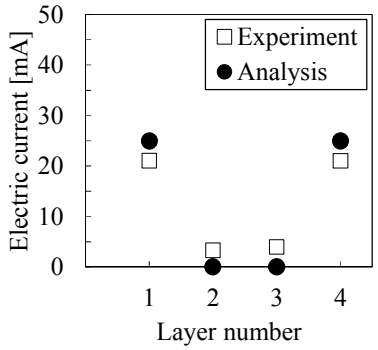

Fig.20 Comparison of i_x of experimental results with that obtained using the oblique flow analysis method for unidirectional laminate

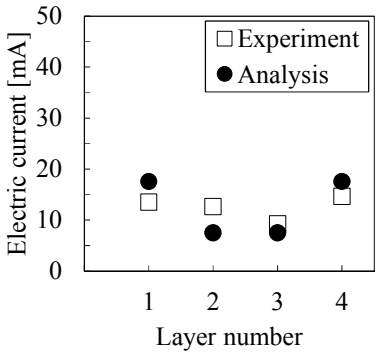

Fig.21 Comparison of i_x of experimental results with that obtained using the oblique flow analysis method for cross-ply laminate.

Plate current analysis

Figure 22 shows the results of the comparison of ix of $[0_{10}]_T$ between the FDM and the new analysis. The abscissa is the distance from the surface in the though-thickness direction. The ordinate is the electric current density. The solid curve gives the results of the new analysis and the open square symbols are the results of FDM computations.

Figures 23 shows the results from $[0/45/-45/90/0]_S$. In this case, ±45°-plies are coupled into a ply that has double-thickness ±45°-ply. The results of the new analysis show good agreement with the results of FDM, and the coupling of ±45°-plies into a ±45°-ply of double-thickness gives a good approximation of electric current density.

Figures 14 shows the results of $[0/45/90/-45/0]_S$. In this case, 45°-, 90°- and −45°-plies are combined and the electric current density results were calculated using the new method and compared with the computational results obtained using FDM. The results of the new analysis give good agreement with the results of FDM.

These results indicate that the approximation of the coupling of three plies, including angle plies, into one orthotropic ply is quite effective for the analysis of electric current density.

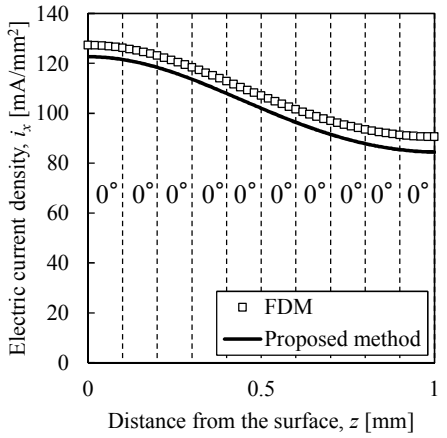

Fig.22 Comparison of results from analysis and FDM computations for the laminate $[0_{10}]_T$ at the origin.

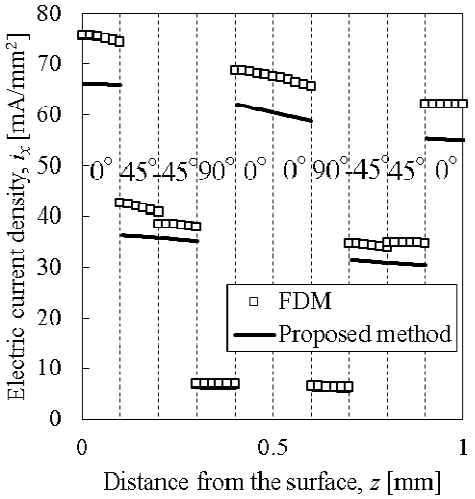

Fig.23 Comparison of results from analysis and FDM computations for the laminate [0/45/−45/90/0]s at the origin.

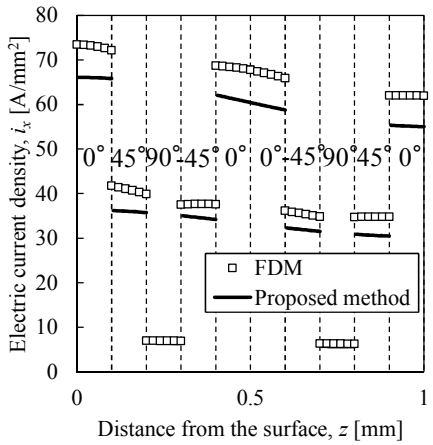

Fig.24 Comparison of results from analysis and FDM computations for the laminate [0/45/90/−45/90]s.

Delamination analysis

Contour diagrams (Figure 25) show the results of analysis for the change in electric potential on the top surface for line source models. These figures show that both results of the doublet-analysis method and FEM agree well. The x-axis profiles for the change in electric potential at $y = z = 0$ are shown in Figure 26. Every result shows that the obtained curve agrees well. The doublet-analysis method is proven to be effective in calculating the change in electric potential induced by the delamination cracks even for the case of line source. This successful results will lead to the next step analysis of the laminates with ACN for delamination detection.

In terms of calculation time, the doublet-analysis method took 4 seconds whereas the FEM took 386 seconds using the same computer. The doublet-analysis therefore demonstrates great efficacy and efficiency over the FEM, although the calculated results show almost the same values.

The doublet-analysis method was proven to be effective for the calculation of electric potential change induced by the delamination cracks, and for shortening the calculation time. To calculate the change in potential, the doublet-analysis method does not need to divide the whole analytical model into small elements, which is necessary in the FEM approach. The advantage of the proposed method, therefore, would be more outstanding in dealing with a model of larger scale. The doublet analysis may enable us to calculate the potential difference caused by delamination cracks for laminates with angled plies, which is still difficult for conventional FEM. This will be our future work.

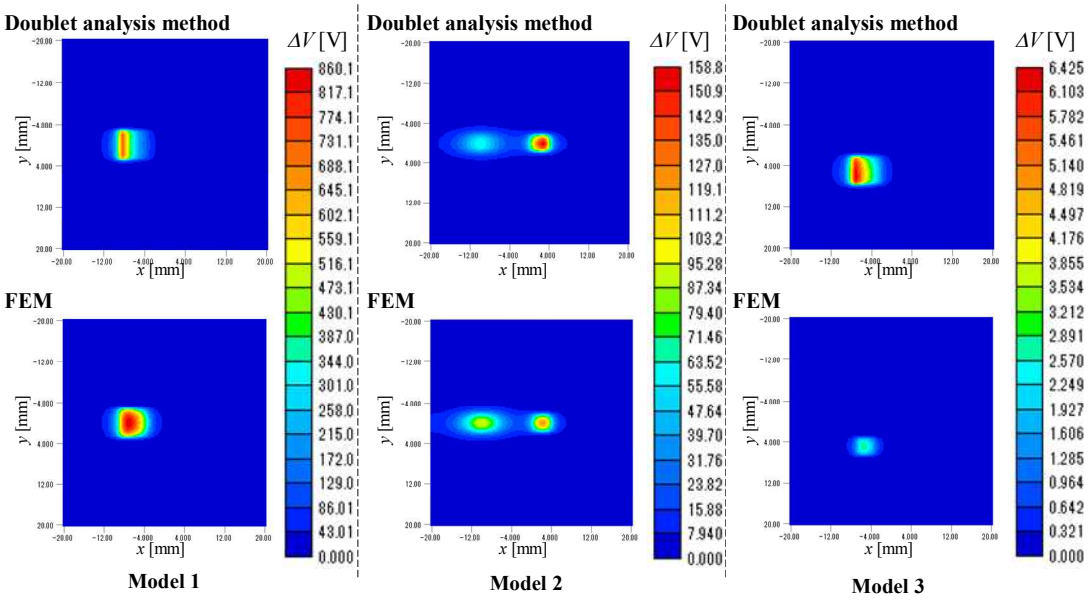

Figure 25. Contour diagrams of calculated results for the change in electric potential induced by delamination cracks on the top surface.

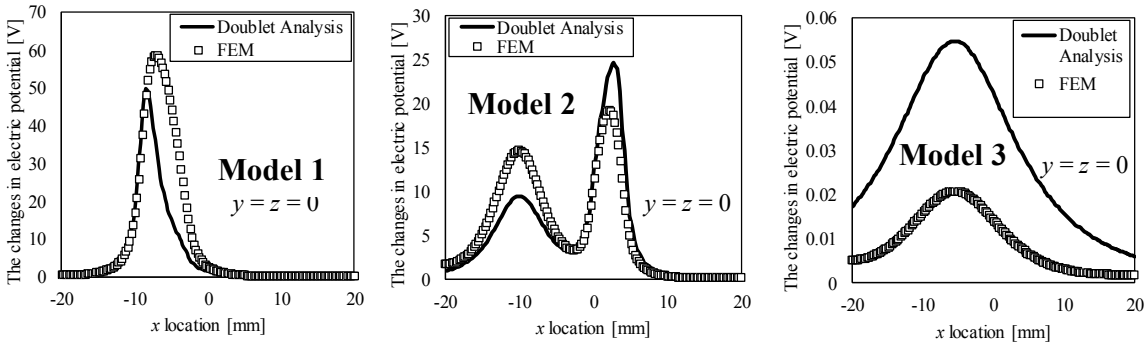

Figure 26. Detailed profile of the change in electric potential along the *x*-axis for the three models.

Summary

Using the newly developed anisotropic potential function, a novel method to evaluate the potential change of the CFRP laminate structure such as the CAN was established. Although the new method is limited to flat plates, there is no large difference of the electric current results between the flat plate and curved structures of laminated CFRP from the electrical resistance change point of view. Especially, for large CFRP structures, we can assume the actual small curvature structures as flat plates. The results obtained in this research, therefore, are indispensable for future research on CFRP self-sensing structure.

References
1. Hojo M, Matsuda S, Tanaka M, Ochiai S, Murakami A. Mode I delamination fatigue properties of interlayer-toughened CF/epoxy laminates. Composites Science and Technology 2006;66(5);665-675.
2. Hirano Y, Katsumata S, Iwahori Y, Todoroki A. Artificial lightning testing on graphite/epoxy composite laminate. Composites: Part A 2010;41(10);1461-1470.
3. Ogasawara T, Hirano Y, Yoshimura A. Coupled thermal-electrical analysis for carbon fiber/epoxy composites exposed to simulated lightning current. Composites: Part A 2010;41(8);973-981.
4. Gagne M, Therriault D. Lightning strike protection of composites. Progress in Aerospace. 2014;64;1-16.
5. Feraboli P, Miller M. Damage resistance and tolerance of carbon/epoxy composite coupons subjected to simulated lightning strike. Composites: Part A 2009;40(6-7);954-967.
6. Abdelal G, Murphy A. Nonlinear numerical modelling of lightning strike effect on composite panels with temperature dependent material properties. Composite Structures 2014;109;268-278.
7. Todoroki A. Electric Current Analysis of CFRP using Perfect Fluid Potential Flow. Transactions of the Japan Society for Aeronautical and Space Sciences 2012;55(3);183-190.
8. Todoroki A. New analytical method for electric current and multiple delamination cracks for thin CFRP cross-ply laminates using equivalent electric conductance. Advanced Composite Materials 2016;25(1);87-101.
9. Yamane T, Todoroki A, Fujita H, Kawashima A, Sekine N. Electric current distribution of carbon fiber reinforced polymer beam: analysis and experimental measurements. Advanced Composite Materials 25,6,(2016)pp. 497-513.
10. Takahashi K, Park JS, Hahn HT. An addressable conducting network for autonomic structural health management of composite structures. Smart materials and structures 2010;19(10);1050-1060.
11. Selvakumaran L, Long Q, Prudhomme S, Lubineau G. On the detectability of transverse cracks in laminated composites using electrical potential change measurements. Composite Structures. 2015;121;237-246.
12. Katz J, Plotkin A. Low-speed aerodynamics: second edition. New York, NY: Cambridge University Press, 2011.
13. Todoroki A, Arai M. Simple electric-voltage-change-analysis method for delamination of thin CFRP laminates using anisotropic electric potential function. Advanced Composite Materials 2014;23(3);261-273.
14. Todoroki A. Electric Current Analysis for Thick Laminated CFRP Composites. Transactions of the Japan Society for Aeronautical and Space Sciences 2012;55(4);237-243.

List of Publications and Significant Collaborations that resulted from your AOARD supported project: In standard format showing authors, title, journal, issue, pages, and date, for each category list the following:

a) papers published in peer-reviewed journals,

[1] Takuya Yamane, Akira Todoroki
Electric potential function of oblique current in laminated carbon fiber reinforced polymer composite beam, Composite Structures 148 (2016) 74-84.
[2] Takuya Yamane and Akira Todoroki
Analysis of electric current density in carbon fiber reinforced plastic laminated plates with angled plies, Composite Structures, 166 (2017), 268-276.
[3] Takuya Yamane, Akira Todoroki
Doublet analysis of changes in electric potential induced by delamination cracks in carbon fiber composite laminates, Composite Structures, 176, (2017)217 - 224

Attachments: The three papers listed above are attached.

DD882: As a separate document, please complete and sign the inventions disclosure form.